# Impact of Starting Model on Waveform Inversion in Ultrasound Tomography

Rehman Ali*, Trevor Mitcham*, and Nebojsa Duric*

*Department of Imaging Sciences, University of Rochester Medical Center, Rochester, NY, 14620 USA

## ABSTRACT

The convergence of waveform inversion in ultrasound tomography is heavily impacted by the choice of starting model. Ray tomography is often used as the starting model for waveform inversion; however, artifacts resulting from ray tomography can continue to persist during waveform inversion. On the other hand, a homogeneous starting model for waveform inversion may result in cycle skipping artifacts if the frequency of the transmitted waveform is too high or the error between the starting model and ground-truth is too large. Clinical in vivo breast data suggests that waveform inversion from a homogeneous starting model is sufficient for an accurate reconstruction of the speed of sound if the starting model is close enough to the average speed of sound in the medium and the starting frequency for waveform inversion is sufficiently low to avoid cycle skipping. Comparing the results of waveform inversion using ray tomography and a homogeneous sound speed as initial models, the homogeneous starting model avoids oscillatory artifacts produced by ray tomography at the edges of the breast. Although the RMS error between the two waveform inversion results is 29.6 m/s, most of the error is the result of reconstruction artifacts at the edges of the breast. When the RMS error is measured inside the breast away from its boundaries, this RMS error drops down to 11.5 m/s.

**Keywords:** Nonlinear inverse problems, waveform inversion, ultrasound, tomography

## 1. INTRODUCTION

Ultrasound tomography (UST) is an imaging technique that uses the transmission of ultrasound through tissue to reconstruct high-resolution images of tissue properties such as sound speed and attenuation. The primary application of ultrasound tomography is in breast imaging[1–6] where sound speed and attenuation are key biomarkers for the identification of cancer in the breast. This report specifically investigates UST for sound speed estimation in heterogeneous sound-speed media.

Techniques for sound speed estimation strategies generally fall into two broad categories: bent-ray methods,[7,8] and waveform inversion.[9,10] Waveform inversion appears to be the most accurate technique for UST reconstruction and greatly outperforms bent-ray reconstructions in most applications. Despite the substantially lower computation time of bent-ray methods, their key drawback is the inability to account for diffraction, which inevitably leads to poorer resolution in the reconstructed image. Waveform inversion is more accurate because it uses iterative simulations of diffraction to estimate the sound speed profile responsible for producing the measured ultrasound signals.

While waveform inversion is the clinical in vivo gold standard for obtaining high-resolution diagnostic-quality images of the speed of sound in tissue,[11,12] it remains unclear to what extent the starting model for the sound speed profile in the medium impacts the solution of waveform inversion. In a ring array geometry, a refraction-corrected bent ray tomography is often used in ultrasound tomography to obtain a starting model prior to waveform inversion.[13] However, similar bent-ray methods were never used in a plane-wave pitch-catch setup; they instead relied on a paraxial approximation of the Helmholtz equation to perform waveform inversion.[14] This brings up several questions: 1) When does bent-ray tomography become necessary to provide a starting model for waveform inversion? 2) What imaging conditions (e.g., frequency band, ring array size) allow for the

Further author information: (Send correspondence to Rehman Ali)
Rehman Ali: E-mail: rali8@stanford.edu

Medical Imaging 2023: Ultrasonic Imaging and Tomography, edited by Christian Boehm, Nick Bottenus, Proc. of SPIE Vol. 12470, 124700J
 · 1605-7422 · doi: 10.1117/12.2653575

waveform inversion reconstruction of the speed of sound from a homogeneous starting model? 3) What range of initial sound speed values work best when starting with a homogeneous model? The purpose of this work is to answer these questions in the context of clinical whole-breast ultrasound tomography with a ring array.

## 2. METHODS

### 2.1 Time-of-Flight Picker and Bent-Ray Tomography

We require measurements of the time of flight to reconstruct the speed of sound using bent ray tomography. The time-of-flight is extracted from the raw ultrasound waveform by finding the time at first break using the Akaike Information Criterion (AIC).[15] The time of flight is then used to reconstruct the speed of sound using a refraction-corrected bent ray tomography with the open-source Bayesian approach described in Ali et al.[16]

### 2.2 Waveform Inversion Using the Helmholtz Equation

Using finite difference methods,[17] we solve the 2D Helmholtz equation to obtain a pressure field $\mathbf{u}$ for a given source $\delta$, frequency $\omega = 2\pi f$, and slowness $\mathbf{s}$ (i.e., the reciprocal of sound speed):

$$(\nabla^2 + \omega^2 \mathbf{s}^2)\mathbf{u}(\omega, \mathbf{s}) = \delta(\omega), \tag{1}$$

After discretization, the $(\nabla^2 + \omega^2 \mathbf{s}^2)$ operator becomes a sparse matrix A that encodes the finite difference scheme so that equation (1) can be described using the following matrix-vector formulation (where $\mathbf{u}$ and $\delta$ are now vectors over spatial locations on the discretized grid):

$$A(\omega, \mathbf{s})\mathbf{u}(\omega, \mathbf{s}) = \delta(\omega), \tag{2}$$

Differentiating both sides of this equation with respect to s gives us:

$$\frac{\partial \mathbf{u}}{\partial \mathbf{s}} = -A^{-1}\frac{\partial A}{\partial \mathbf{s}}\mathbf{u} = -A^{-1}\frac{\partial A}{\partial \mathbf{s}}A^{-1}\delta, \tag{3}$$

Rather than observing the full pressure field $\mathbf{u}$ at all locations in space, we only observe the pressure field $\mathbf{p}$ at the ring array. The relationship between $\mathbf{p}$ and $\mathbf{u}$ is: $\mathbf{p} = K\mathbf{u}$, where K is a sampling operator that extracts the pressure field at each element of the ring array. The relationship between changes in slowness and changes in the simulated pressure field at the ring array is

$$\frac{\partial \mathbf{p}}{\partial \mathbf{s}} = -KA^{-1}\frac{\partial A}{\partial \mathbf{s}}\mathbf{u} = -KA^{-1}\frac{\partial A}{\partial \mathbf{s}}A^{-1}\delta, \tag{4}$$

The cost function for waveform inversion is:

$$E(\omega, \mathbf{s}) = \frac{1}{2}\sum_{i=1}^{N}\|\mathbf{p_i}(\omega, \mathbf{s}) - \mathbf{p_{obs,i}}(\omega)\|_2^2 = \frac{1}{2}\sum_{i=1}^{N}\left(\mathbf{p_i}(\omega, \mathbf{s}) - \mathbf{p_{obs,i}}(\omega)\right)^H\left(\mathbf{p_i}(\omega, \mathbf{s}) - \mathbf{p_{obs,i}}(\omega)\right), \tag{5}$$

where $\mathbf{p_i}$ and $\mathbf{p_{obs,i}}$ are the simulated and observed pressure measurements on the ring array for the $i^{th}$ single-element transmission $\delta_\mathbf{i}$ (i ranges from 1 to N, the number of elements on the ring array). The gradient of $E(\omega, \mathbf{s})$ with respect to slowness $\mathbf{s}$ is given by:

$$\nabla_\mathbf{s} E = \sum_{i=1}^{N} Re\left\{\left(\frac{\partial \mathbf{p_i}}{\partial \mathbf{s}}\right)^H(\mathbf{p_i} - \mathbf{p_{obs,i}})\right\} = -\sum_{i=1}^{N} Re\left\{\left(\frac{\partial A}{\partial \mathbf{s}}\mathbf{u_i}\right)^H(A^H)^{-1}K^T(\mathbf{p_i} - \mathbf{p_{obs,i}})\right\}, \tag{6}$$

To implement the conjugate gradient method for this objective function, we also need a linear estimate of the perturbation in the pressure field $\Delta\mathbf{p_i}$ for a given perturbation $\mathbf{d_k}$ to the slowness.

$$\Delta\mathbf{p_i} = \left(\frac{\partial \mathbf{p_i}(\omega, \mathbf{s})}{\partial \mathbf{s}}\right)\mathbf{d_k} = -KA(\omega, \mathbf{s})^{-1}\left(\frac{\partial A(\omega, \mathbf{s})}{\partial \mathbf{s}}\mathbf{u_i}(\omega, \mathbf{s})\right)\mathbf{d_k}. \tag{7}$$

This perturbation $\Delta\mathbf{p_i}$ allows us to properly scale the search direction $\mathbf{d_k}$ and update the slowness model $\mathbf{s_k}$:

$$\alpha_k = -\frac{\mathbf{d_k}^T\nabla_\mathbf{s}E}{\|\Delta\mathbf{p_i}\|_2^2} \tag{8}$$

$$\mathbf{s_{k+1}} = \mathbf{s_k} + \alpha_k\mathbf{d_k} \tag{9}$$

Note that first iteration of conjugate gradient is simply direct gradient descent (i.e., $d_1 = -\nabla_\mathbf{s}E(\omega, \mathbf{s})$).

### 2.3 Complex-Valued Source Scaling

The waveform inversion described in the previous section assumes that the correct phase and amplitude is used for each single-element source $\delta_{\mathbf{i}}$; however, in practice, the phase and amplitude of each source must be estimated from measured waveform. The following projection formula provides a complex scaling $\gamma_i$ that accounts for both the amplitude and phase from each source $i$:

$$\gamma_i = \frac{\mathbf{p_i}^H \mathbf{p_{obs,i}}}{\mathbf{p_i}^H \mathbf{p_i}} \tag{10}$$

The source vector and pressure fields are scaled to $\{\delta_{\mathbf{i}} \rightarrow \gamma_i \delta_{\mathbf{i}}\}$, $\{\mathbf{u_i} \rightarrow \gamma_i \mathbf{u_i}\}$, and $\{\mathbf{p_i} \rightarrow \gamma_i \mathbf{p_i}\}$, respectively.

### 2.4 Numerical Simulations

Figure 1 shows (a) the ground-truth sound speed map for a numerical breast phantom derived from a contrast-enhanced cone-beam breast CT image in work from the Diagnostic Breast Center Göttingen (https://doi.org/10.1016/j.tranon.2017.08.010)[18] under the Creative Commons Attribution-NonCommercial-No Derivatives License (CC BY NC ND) (https://creativecommons.org/licenses/by-nc-nd/4.0/), and (b) the ground-truth sound speed map for the a numerical breast phantom derived from a 3D breast MRI dataset.[19]

For the k-Wave simulation[20] involving the numerical breast phantom in Figure 1(a), single-element transmissions with 2.5 MHz center frequency (75% fractional bandwidth) were simulated from an 11 cm diameter ring array with 256 elements. For the k-Wave simulation involving the numerical breast phantom in Figure 1(b), single-element transmissions with 1.0 MHz center frequency (75% fractional bandwidth) were simulated from an 22 cm diameter ring array with 512 elements. Received channel data (time traces for the received signal from each individual element for each single-element transmission) from these k-Wave simulations were used to reconstruct the sound speed in the medium using the previously described waveform inversion algorithm. No noise was added to the received channel data simulated in k-Wave.

For case (a), waveform inversion used frequencies ranging from 0.5 to 1.5 MHz in 50 kHz steps starting from an initial homogeneous sound speed of 1515 m/s. The starting frequency was increased from 0.5 to 1.05 MHz in 50 kHz steps to assess how the starting frequency impacts cycle skipping. For case (b), waveform inversion used frequencies ranging from 0.3 to 0.7 MHz in 50 kHz steps starting from initial homogeneous sound speeds ranging from 1400 to 1540 m/s to assess convergence from a range of initial sound speed values when starting with a homogeneous model. In each case, 3 iterations of conjugate gradient were used at each frequency.

### 2.5 Experiments

Raw ultrasound channel data from a whole-breast ultrasound tomography system (Delphinus Medical Technologies Inc., Novi, MI) was used to reconstruct the speed of sound in the breast (data collected under IRB No. 040912M1F). The Delphinus ultrasound tomography system consists of a 22 cm diameter ring transducer with 1024 elements and a pulse center frequency of 2.5 MHz. In each experiment, waveform inversion, using frequencies ranging from 0.3 to 1.25 MHz, is used to reconstruct the sound speed starting from a homogeneous model of 1480 m/s. Waveform inversion is also used to reconstruct the speed of sound by using ray tomography as the starting model. In each case, 3 iterations of conjugate gradient were used at each frequency.

## 3. RESULTS

Figure 2 shows how cycle skipping enters the final image reconstruction as the starting frequency used in waveform inversion is gradually increased. As the starting frequency is increased from 0.5 to 1.05 MHz in 50 kHz steps, cycle skipping begins to first appear at 0.7 MHz. As the starting frequency is increased beyond 0.7 MHz the strength and severity of cycle skipping artifacts increase. This initial k-Wave simulation of a 11 cm diameter ring array system is used to quickly show the impact of starting frequency on wwveform inversion. The next set of k-Wave simulations for a 22 cm diameter ring array are used to better replicate the frequency and initial sound speed dependence found in the experimental acquisition system: Figures 3, 4, and 5 shows the dependence of cycle skipping on the choice of the initial homogeneous sound speed model at starting frequencies of 0.3, 0.4, and 0.5 MHz, respectively. As the starting frequency increases, the range of initial homogeneous sound speed models

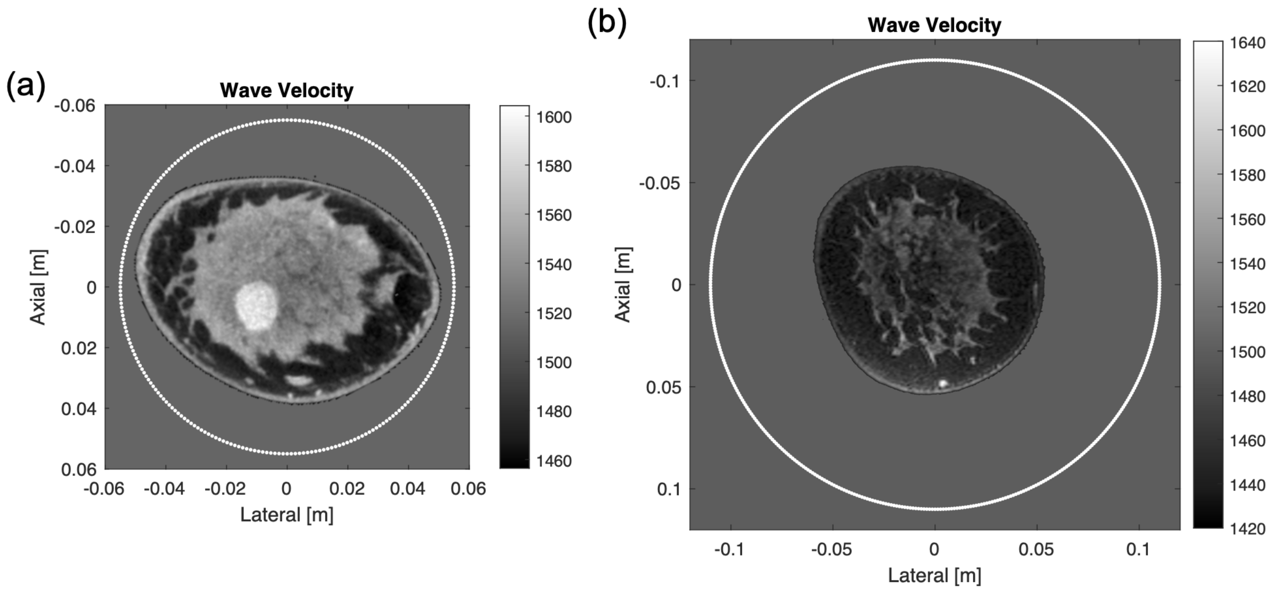


Figure 1. Sound Speed Maps [m/s] for Numerical Breast Phantoms. (a) Sound speed map for 11 cm diameter ring array (256 elements) k-Wave simulation was adapted and modified from a contrast-enhanced cone-beam breast CT image in work from the Diagnostic Breast Center Göttingen (https://doi.org/10.1016/j.tranon.2017.08.010)[18] under the Creative Commons Attribution-NonCommercial-No Derivatives License (CC BY NC ND) (https://creativecommons.org/licenses/by-nc-nd/4.0/). (b) Sound speed map for 22 cm diameter ring array (512 elements) k-Wave simulation was adapted from 3D breast MRI dataset.[19]

from which convergence may be achieved becomes increasingly narrow. At a starting frequency of 0.5 MHz, no choice of initial homogeneous sound speed model will avoid cycle skipping, but the effects of cycle skipping appear to be minimized using an initial homogeneous model having a sound speed of around 1475 m/s.

Figure 6 shows the result of applying waveform inversion to breast ultrasound data from a ring array transducer with and without ray tomography as a starting model. Ray tomography provides the general shape and sound speed profile of the breast with oscillations occurring at the interface between the water bath and the breast. These artifactual oscillations are the result of applying ray tomography when there is a sharp transition in the speed of sound. Using ray tomography as the starting model, waveform inversion improves resolution and better visualizes the true boundary between the breast and background water bath; however, the artifactual oscillations observed in the ray reconstruction continue to persist after waveform inversion. Instead, if we start with a 1480 m/s homogeneous initial model, we avoid these artifacts at boundaries of the breast and see much better visualization and resolution of internal structures within the breast. Because of the error between the 1480 m/s initial model and the speed of sound in the water bath, there is a halo effect near the ring in this reconstruction. By starting waveform inversion at 0.3 MHz and providing an initial homogeneous sound speed of 1480 m/s (close to the combined mean sound speed between the breast and water bath), waveform inversion avoids cycle skipping and circumvents the need for ray tomography to provide a starting model. The RMS error between the two waveform inversion reconstructions (measured inside the region bounded by the ring array) is 29.6 m/s. However, this large error is mainly the result of the ray tomography artifacts at the edges of the breast. Instead, if we choose a 4 cm radius region-of-interest inside the breast, the RMS error in the reconstruction reduces to 11.5 m/s. Furthermore, it is unclear whether the artifacts at the edges of the breast are the result of out-of-plane scattering, which our two-dimensional implementation of the Helmholtz equation does not take into account. Our second *in vivo* example (Figure 7) shows that while cycle skipping can still be avoided by using an adequate homogeneous starting model at a sufficiently low frequency, ray tomography can still fill certain null region of the image caused by outliers in the channel data.

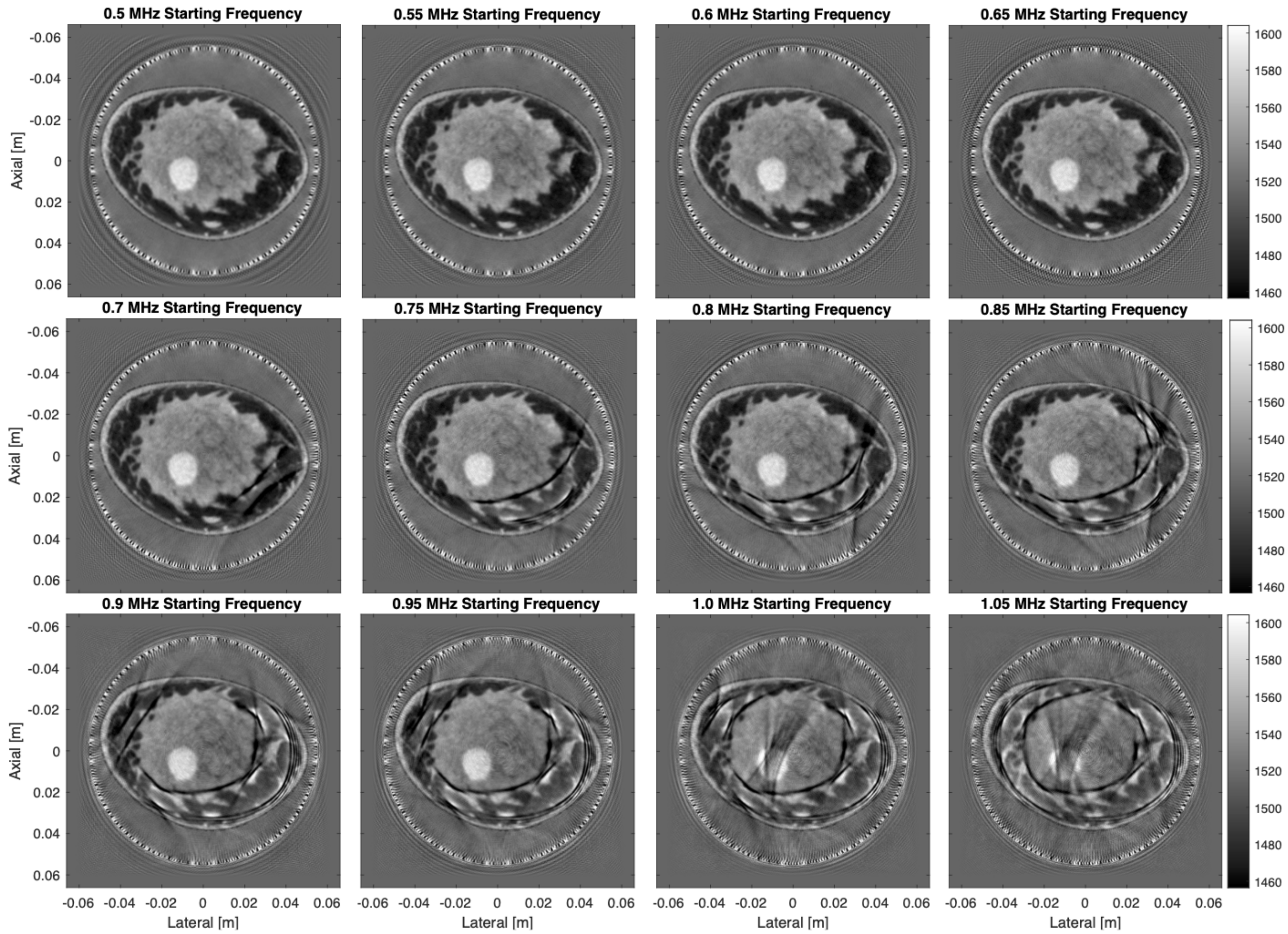


Figure 2. Cycle Skipping as a Function of Increasing Starting Frequency. In each case, waveform inversion is stepped from the starting frequency to 1.5 MHz in 50 kHz steps. Up to a 0.65 MHz starting frequency, cycle skipping is not observed in the final reconstruction. The first cycle skipping artifact appear in the final reconstruction when the starting frequency is set to 0.7 MHz. The strength and severity of the cycle skipping artifact increases with frequency.

## 4. DISCUSSION AND CONCLUSIONS

Ultimately, the goal of this paper is to answer three important questions in the context of waveform inversion for a ring array breast ultrasound tomography system: 1) When does bent-ray tomography become necessary to provide a starting model for waveform inversion? 2) What imaging conditions (e.g., frequency band, ring array size) allow for the waveform inversion reconstruction of the speed of sound from a homogeneous starting model? 3) What range of initial sound speed values work best when starting with a homogeneous model?.

We first investigate question (2) and observe that cycle skipping is primarily a function of the starting frequency used in waveform inversion. Artifact appear to increase as the starting frequency increases. When doubling the size of the ring from case (a) to case (b) in Figure 1, the starting frequencies at which cycle skipping artifacts appear in the images is approximately halved. Conceptually this make sense because the frequency would need to be halved for the accumulated phase shift to remain roughly the same over double the distance. When investigating the question (3), we find that the range of initial sound speed when using a homogeneous starting model is impacted by the choice of starting frequency and show that the range of starting sound speeds from which convergence is achieved becomes increasingly narrow as the frequency increases (Figures 3, 4, and 5).

Lastly, we directly investigate question (1) by using ray tomography and waveform inversion in two different *in vivo* examples (Figure 6 and 7). These example show that while waveform inversion can avoid cycle skipping

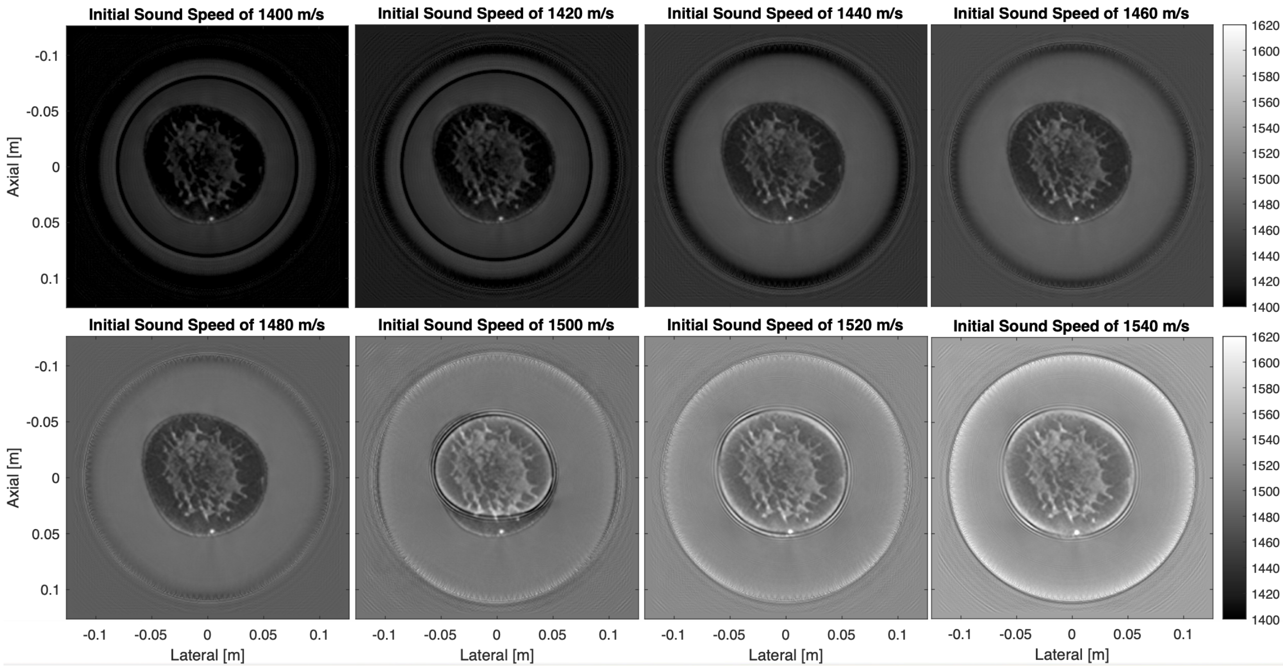


Figure 3. Impact of Homogeneous Starting Model at Starting Frequency of 0.3 MHz. In each case, waveform inversion is stepped from 0.3 to 0.7 MHz in 50 kHz steps. A starting sound speed model ranging from 1440 to 1480 m/s appears to avoid cycle skipping when starting waveform inversion at 0.3 MHz.

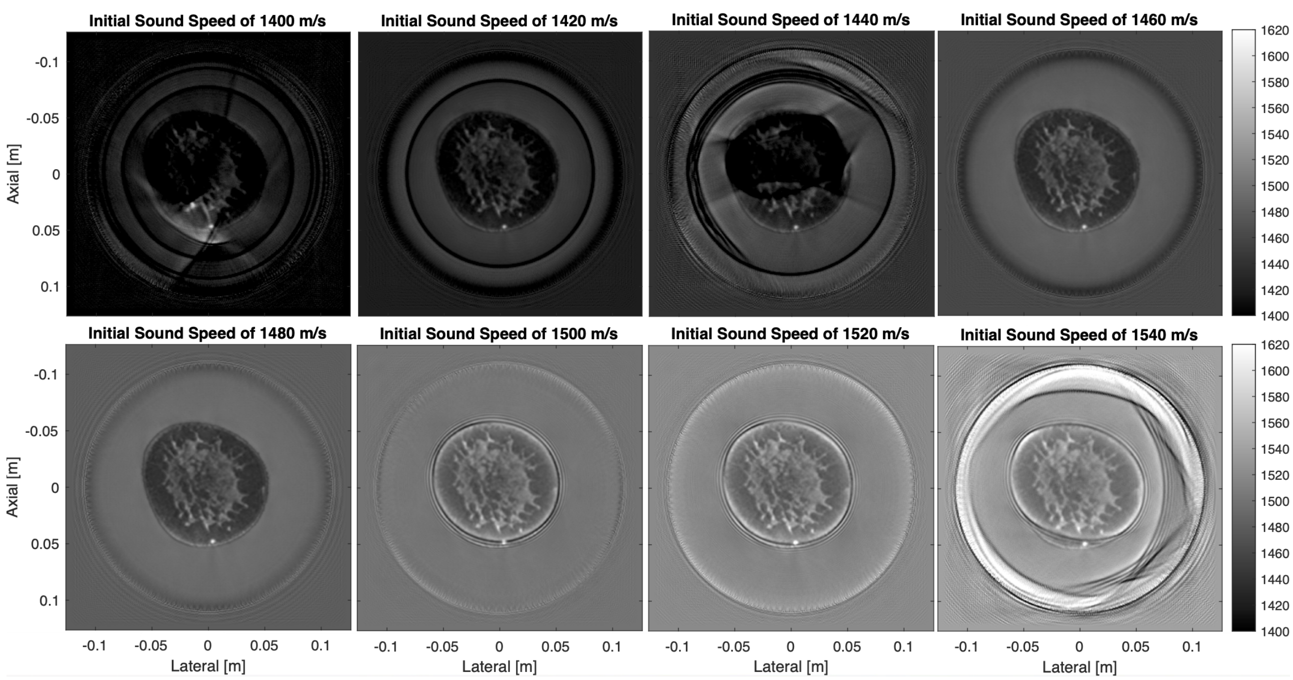


Figure 4. Impact of Homogeneous Starting Model at Starting Frequency of 0.4 MHz. In each case, waveform inversion is stepped from 0.4 to 0.7 MHz in 50 kHz steps. A starting sound speed model ranging from 1460 to 1480 m/s appears to avoid cycle skipping when starting waveform inversion at 0.4 MHz.

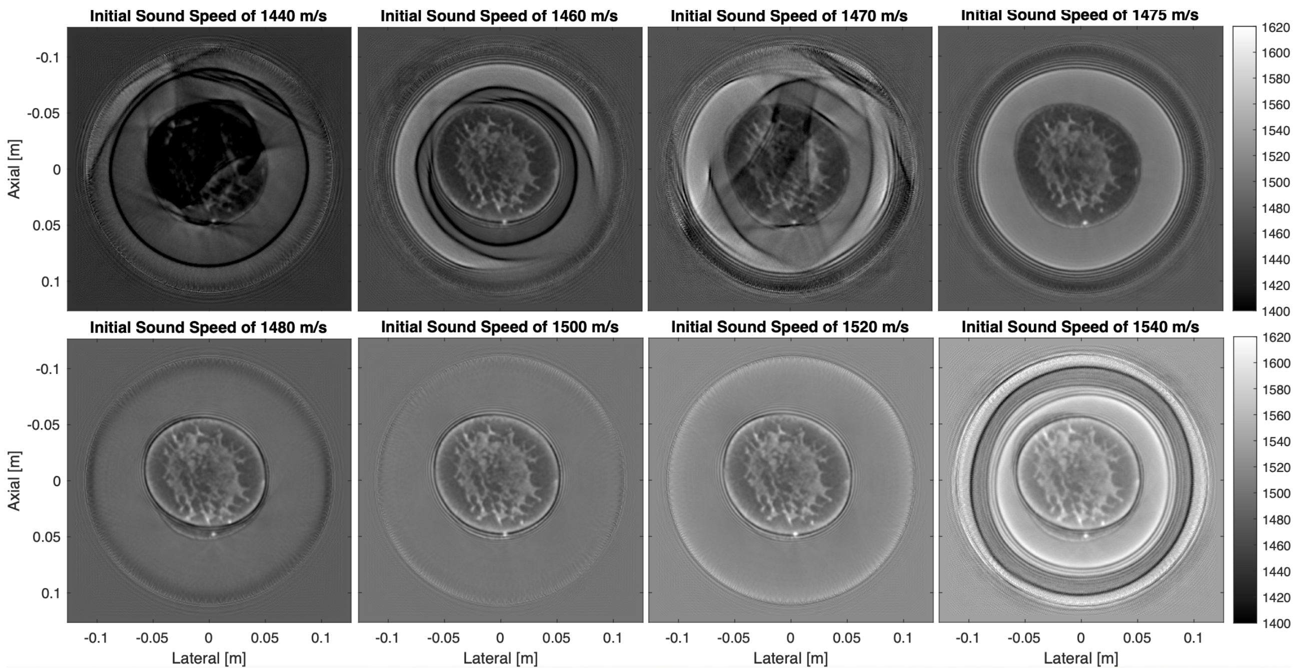


Figure 5. Impact of Homogeneous Starting Model at Starting Frequency of 0.5 MHz. In each case, waveform inversion is stepped from 0.5 to 0.7 MHz in 50 kHz steps. A starting sound speed model of 1475 m/s appears to minimize the effect of cycle skipping on the breast reconstruction when starting waveform inversion at 0.5 MHz. However, cycle skipping is present for every choice of homogeneous starting model when starting waveform inversion at 0.5 MHz.

provided that the starting frequency is sufficiently low and the initial sound speed guess is sufficiently close to the global average sound speed in the medium, ray tomography adds a significant amount of prior information. In the first example (Figure 6), ray tomography has a significant impact on the reconstruction near the surface of the breast, but it is unclear whether this can be considered an improvement in image quality. In the second example (Figure 7), ray tomography helps fill outliers in the channel data that waveform inversion was not able to fill on its own. However, these same outlier regions could also be smoothed over using regularization. Regularization is not typically used in waveform inversion for ultrasound tomography because waveform inversion typically covers all the pixels in the sound speed distribution and does not have the same model sparsity issues found in ray tomography. However, future work may still consider the use of regularization to eliminate outliers.

This investigation ultimately assesses many of the parameters that go into the design of a waveform inversion tomography system. The choice of hardware ultimately limits the frequency range and size of the imaging system. A larger ring array will typically need lower frequencies to avoid cycle skipping, but in many cases, the ultrasound transducer may not have a sufficiently broad bandwidth to cover the low frequencies used in this study. In those cases, a ray tomography is extremely important as a starting model. One parameter that was not explicitly shown in this study was the use of bent-ray vs straight-ray tomography as a starting model. When using a straight-ray reconstruction in lieu of the bent-ray reconstruction as the starting model in Figure 7, the end result of waveform inversion is practically identical. This means that bent-ray tomography (and ray tracing via the eikonal equation) is not strictly necessary for waveform inversion. A straight ray tomography appears to be sufficient as a starting model for waveform inversion when applied to breast imaging. Future work should investigate methodologies that eliminate the need for ray tomography by overcoming cycle skipping effects altogether[21–23] as well as reduce the impact of out-of-plane artifacts by using a 3D reconstruction model.[24,25]

## ACKNOWLEDGMENTS

The authors would like to acknowledge Dr. Cuiping Li at Delphinus Medical Technologies for her valuable input and advice on this work. The authors would also like to thank Electrical Engineering PhD student Thurston

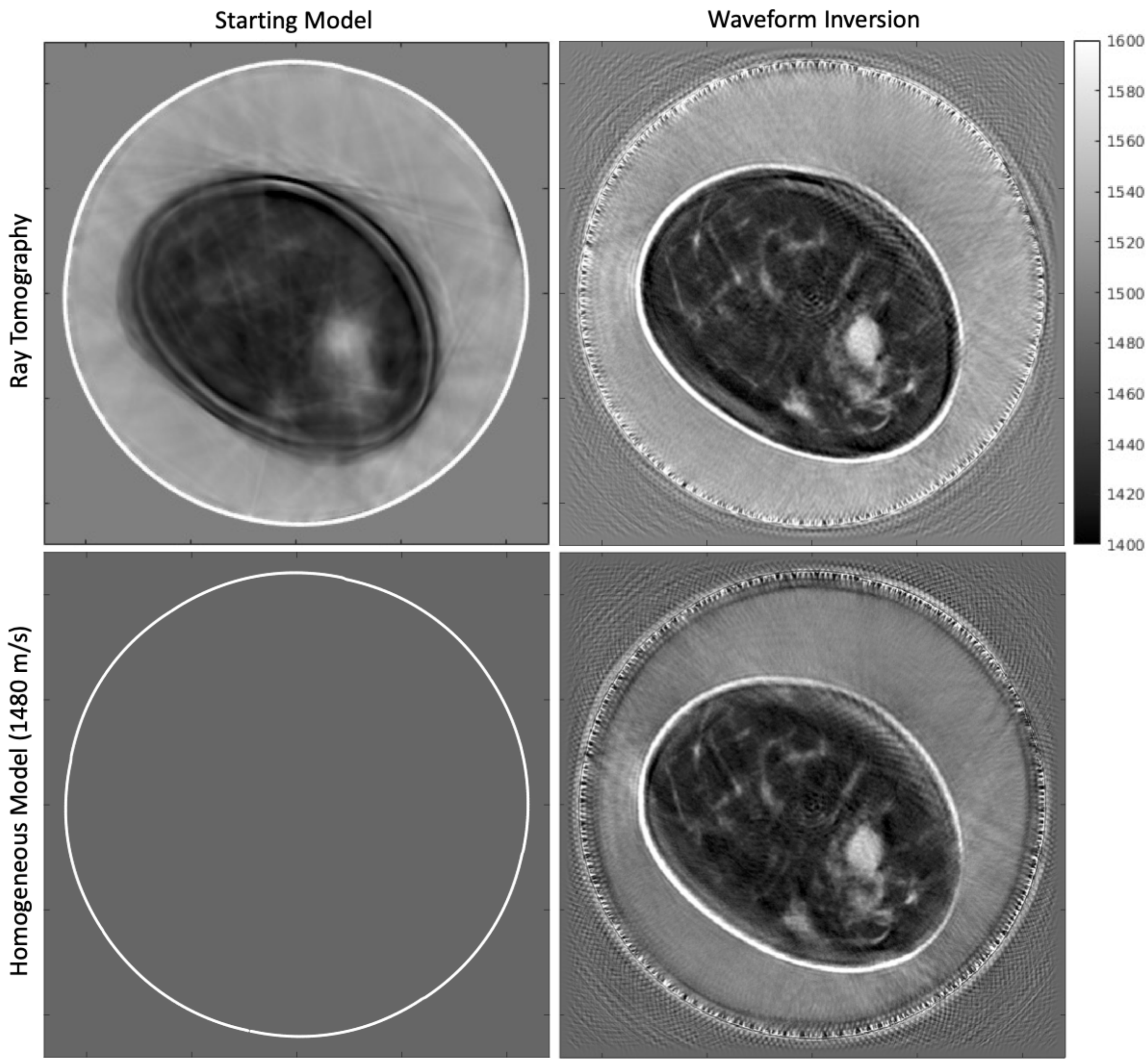


Figure 6. First *In-Vivo* Example of Waveform Inversion Reconstruction of the Speed of Sound With and Without Ray Tomography as a Starting Model. Ray tomography has artifactual oscillations near the boundary of the breast. Although waveform inversion improves imaging resolution and better visualizes the actual boundary of the breast, the oscillatory artifacts produced by the ray tomography still remains after applying waveform inversion. On the other hand, waveform inversion starting from a homogeneous model (1480 m/s) avoids these artifacts, and cycle skipping is avoided by starting waveform inversion at a low frequency of 0.3 MHz.

Brevett from Stanford University for helping the authors to optimize their GPU implementation of the Helmholtz equation and waveform inversion routines.

## REFERENCES

[1] Li, C., Duric, N., Littrup, P., and Huang, L., "In-vivo breast sound-speed imaging with ultrasound tomography," *Ultrasound in Medicine and Biology* **35**(10), 1615–1628 (2009).

[2] Duric, N., Littrup, P., Poulo, L., Babkin, A., Pevzner, R., Holsapple, E., Rama, O., and Glide, C., "Detection of breast cancer with ultrasound tomography: First results with the computed ultrasound risk evaluation (CURE) prototype," *Medical physics* **34**(2), 773–785 (2007).

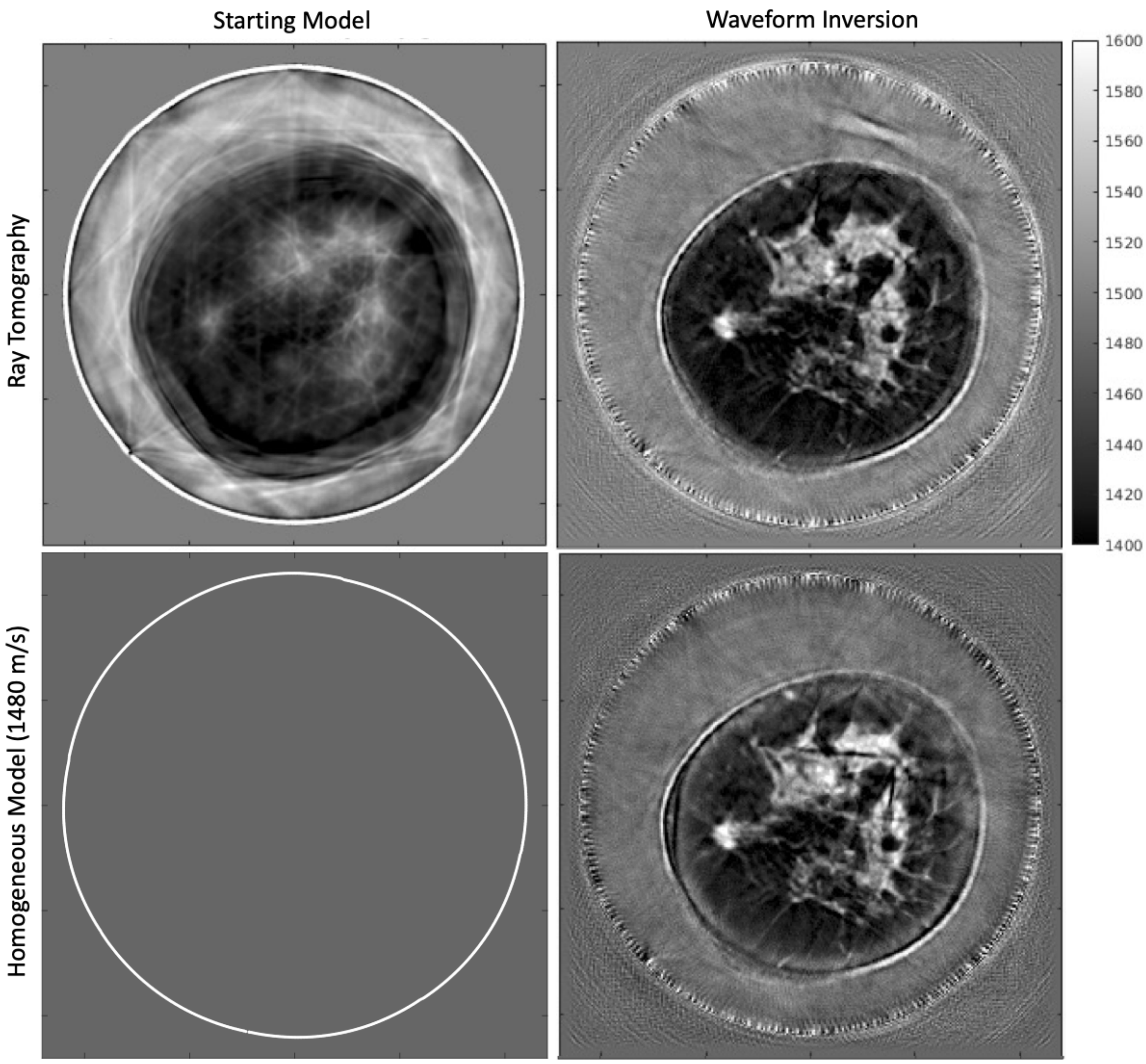


Figure 7. Second *In-Vivo* Example of Waveform Inversion Reconstruction of the Speed of Sound With and Without Ray Tomography as a Starting Model. Although waveform inversion starting from a homogeneous model (1480 m/s) mostly avoids cycle skipping by starting at a low frequency of 0.3 MHz, there is artifactual dropout in parts of the breast image due the outliers in the measured signals used to perform waveform inversion. In this case, ray tomography appears to helps fill certain outlier regions in the final reconstruction that waveform inversion cannot.

[3] Schreiman, J., Gisvold, J., Greenleaf, J. F., and Bahn, R., "Ultrasound transmission computed tomography of the breast.," *Radiology* **150**(2), 523–530 (1984).

[4] Wiskin, J., Borup, D., Johnson, S., and Berggren, M., "Non-linear inverse scattering: high resolution quantitative breast tissue tomography," *The Journal of the Acoustical Society of America* **131**(5), 3802–3813 (2012).

[5] Kolb, T. M., Lichy, J., and Newhouse, J. H., "Occult cancer in women with dense breasts: detection with screening US–diagnostic yield and tumor characteristics.," *Radiology* **207**(1), 191–199 (1998).

[6] Kolb, T. M., Lichy, J., and Newhouse, J. H., "Comparison of the performance of screening mammography, physical examination, and breast US and evaluation of factors that influence them: an analysis of 27,825 patient evaluations," *Radiology* **225**(1), 165–175 (2002).

[7] Hormati, A., Jovanović, I., Roy, O., and Vetterli, M., "Robust ultrasound travel-time tomography using the

bent ray model," in [*Medical Imaging 2010: Ultrasonic Imaging, Tomography, and Therapy*], **7629**, 76290I, International Society for Optics and Photonics (2010).

[8] Quan, Y. and Huang, L., "Sound-speed tomography using first-arrival transmission ultrasound for a ring array," in [*Medical Imaging 2007: Ultrasonic Imaging and Signal Processing*], **6513**, 651306, International Society for Optics and Photonics (2007).

[9] Wang, K., Matthews, T., Anis, F., Li, C., Duric, N., and Anastasio, M. A., "Waveform inversion with source encoding for breast sound speed reconstruction in ultrasound computed tomography," *IEEE transactions on ultrasonics, ferroelectrics, and frequency control* **62**(3), 475–493 (2015).

[10] Krebs, J. R., Anderson, J. E., Hinkley, D., Neelamani, R., Lee, S., Baumstein, A., and Lacasse, M.-D., "Fast full-wavefield seismic inversion using encoded sources," *Geophysics* **74**(6), WCC177–WCC188 (2009).

[11] Sandhu, G., Li, C., Roy, O., Schmidt, S., and Duric, N., "Frequency domain ultrasound waveform tomography: breast imaging using a ring transducer," *Physics in Medicine & Biology* **60**(14), 5381 (2015).

[12] Wiskin, J., Malik, B., Natesan, R., Borup, D., Pirshafiey, N., Lenox, M., and Klock, J., "Full wave 3d inverse scattering transmission ultrasound tomography: breast and whole body imaging," in [*2019 IEEE International Ultrasonics Symposium (IUS)*], 951–958, IEEE (2019).

[13] Li, C., Duric, N., Littrup, P., and Huang, L., "In vivo breast sound-speed imaging with ultrasound tomography," *Ultrasound in medicine & biology* **35**(10), 1615–1628 (2009).

[14] Malik, B., Terry, R., Wiskin, J., and Lenox, M., "Quantitative transmission ultrasound tomography: Imaging and performance characteristics," *Medical physics* **45**(7), 3063–3075 (2018).

[15] Li, C., Huang, L., Duric, N., Zhang, H., and Rowe, C., "An improved automatic time-of-flight picker for medical ultrasound tomography," *Ultrasonics* **49**(1), 61–72 (2009).

[16] Ali, R., Hsieh, S., and Dahl, J., "Open-source gauss-newton-based methods for refraction-corrected ultrasound computed tomography," in [*Medical Imaging 2019: Ultrasonic Imaging and Tomography*], **10955**, 39–52, SPIE (2019).

[17] Chen, Z., Cheng, D., Feng, W., and Wu, T., "An optimal 9-point finite difference scheme for the helmholtz equation with pml.," *International Journal of Numerical Analysis & Modeling* **10**(2) (2013).

[18] Uhlig, J., Fischer, U., von Fintel, E., Stahnke, V., Perske, C., Lotz, J., and Wienbeck, S., "Contrast enhancement on cone-beam breast-ct for discrimination of breast cancer immunohistochemical subtypes," *Translational oncology* **10**(6), 904–910 (2017).

[19] Saha, A., Harowicz, M. R., Grimm, L. J., Kim, C. E., Ghate, S. V., Walsh, R., and Mazurowski, M. A., "A machine learning approach to radiogenomics of breast cancer: a study of 922 subjects and 529 dce-mri features," *British journal of cancer* **119**(4), 508–516 (2018).

[20] Treeby, B. E. and Cox, B. T., "k-wave: Matlab toolbox for the simulation and reconstruction of photoacoustic wave fields," *Journal of biomedical optics* **15**(2), 021314 (2010).

[21] Warner, M. and Guasch, L., "Adaptive waveform inversion: Theory," *Geophysics* **81**(6), R429–R445 (2016).

[22] Guasch, L., Warner, M., and Ravaut, C., "Adaptive waveform inversion: Practice," *Geophysics* **84**(3), R447–R461 (2019).

[23] Guasch, L., Calderón Agudo, O., Tang, M.-X., Nachev, P., and Warner, M., "Full-waveform inversion imaging of the human brain," *NPJ digital medicine* **3**(1), 1–12 (2020).

[24] Sandhu, G. Y., West, E., Li, C., Roy, O., and Duric, N., "3d frequency-domain ultrasound waveform tomography breast imaging," in [*Medical Imaging 2017: Ultrasonic Imaging and Tomography*], **10139**, 56–69, SPIE (2017).

[25] Li, F., Villa, U., Duric, N., and Anastasio, M. A., "Investigation of an elevation-focused transducer model for three-dimensional full-waveform inversion in ultrasound computed tomography," in [*Medical Imaging 2022: Ultrasonic Imaging and Tomography*], **12038**, 206–214, SPIE (2022).